

CERN-EP-2022-220
20 October 2022

Search for the Chiral Magnetic Effect with charge-dependent azimuthal correlations in Xe–Xe collisions at $\sqrt{s_{\text{NN}}} = 5.44$ TeV

ALICE Collaboration

Abstract

Charge-dependent two- and three-particle correlations measured in Xe–Xe collisions at $\sqrt{s_{\text{NN}}} = 5.44$ TeV are presented. Results are obtained for charged particles in the pseudorapidity range $|\eta| < 0.8$ and transverse momentum interval $0.2 \leq p_{\text{T}} < 5.0$ GeV/ c for different collision centralities. The three-particle correlator $\gamma_{\alpha\beta} \equiv \langle \cos(\varphi_{\alpha} + \varphi_{\beta} - 2\Psi_2) \rangle$, calculated for different combinations of charge sign α and β , is expected to be sensitive to the presence of the Chiral Magnetic Effect (CME). Its magnitude is similar to the one observed in Pb–Pb collisions in contrast to a smaller CME signal in Xe–Xe collisions than in Pb–Pb collisions predicted by Monte Carlo (MC) calculations including a magnetic field induced by the spectator protons. These observations point to a large non-CME contribution to the correlator. Furthermore, the charge dependence of $\gamma_{\alpha\beta}$ can be described by a blast wave model calculation that incorporates background effects and by the Anomalous Viscous Fluid Dynamics model with values of the CME signal consistent with zero. The Xe–Xe and Pb–Pb results are combined with the expected CME signal dependence on the system size from the MC calculations including a magnetic field to obtain the fraction of CME contribution in $\gamma_{\alpha\beta}$, f_{CME} . The CME fraction is compatible with zero for the 30% most central events in both systems and then becomes positive; averaging over the 0–70% centrality interval yields an upper limit of 2% (3%) and 25% (32%) at 95% (99.7%) confidence level for the CME signal contribution to $\gamma_{\alpha\beta}$ in Xe–Xe and Pb–Pb collisions, respectively.

arXiv:2210.15383v1 [nucl-ex] 27 Oct 2022

1 Introduction

The theory of the strong interaction applied to many-body systems predicts that, at sufficiently high densities and temperatures, the protons and neutrons that compose ordinary matter melt into a plasma where quarks and gluons are no longer confined into hadrons. This hot and dense state of matter is called the quark–gluon plasma (QGP) [1]. The transition from normal hadronic matter to a QGP is supported by Quantum Chromodynamics (QCD) calculations on the lattice [2–5], where it is found to occur at a critical temperature of about 155 MeV, and at a critical energy density ε of about 0.5 GeV/fm³ [6–8]. Collisions between heavy ions accelerated to ultrarelativistic energies can produce the necessary conditions for such a transition to take place [9–11].

Heavy-ion collisions may also allow us to access novel QCD phenomena associated with parity violation in strong interactions [12–20]. Theoretical expectations indicate that the interaction of quarks with gluonic fields describing transitions between topologically different QCD vacuum states changes the quark chirality and leads to a local chiral imbalance. In the presence of the strong magnetic field produced by the colliding ions [21–23], this leads to a charge separation (electric current) relative to the reaction plane, the plane defined by the impact parameter and the beam axis. This phenomenon is known as the Chiral Magnetic Effect (CME) [20].

The effects from local parity violation are quantified via the coefficient $a_{1,\alpha}$ in a Fourier decomposition of the particle azimuthal distribution [24, 25]

$$\frac{dN}{d\Delta\varphi_\alpha} \sim 1 + 2v_{1,\alpha} \cos(\Delta\varphi_\alpha) + 2a_{1,\alpha} \sin(\Delta\varphi_\alpha) + 2v_{2,\alpha} \cos(2\Delta\varphi_\alpha) + \dots, \quad (1)$$

where $\Delta\varphi_\alpha = \varphi_\alpha - \Psi_{\text{RP}}$, φ_α is the azimuthal angle of the particle of charge α (+, –), and Ψ_{RP} is the reaction plane angle. The coefficients $v_{n,\alpha}$ characterise the anisotropic flow, i.e., the azimuthal anisotropies in particle production relative to Ψ_{RP} due to initial spatial asymmetries of the collision. The degree of overlap between the two colliding nuclei is estimated by the centrality, with low percentage values corresponding to head-on collisions. The first- and second-order flow coefficients ($v_{1,\alpha}$ and $v_{2,\alpha}$) are called directed and elliptic flow, respectively. The CME is expected to have an experimentally accessible signal imprinted in the azimuthal correlations between two particles relative to the reaction plane [25] of the form $\gamma_{\alpha\beta} \equiv \langle \cos(\varphi_\alpha + \varphi_\beta - 2\Psi_{\text{RP}}) \rangle$, since $a_{1,\alpha}$ changes sign from event to event and the average $\langle a_{1,\alpha} \rangle$ over many events is equal to zero. The charge-dependent difference of $\gamma_{\alpha\beta}$ is commonly used to search for the CME. In practice, the reaction plane angle is estimated by constructing the second harmonic symmetry plane angle Ψ_2 using azimuthal particle distributions [26], which is why $\gamma_{\alpha\beta}$ is often referred to as a three-particle correlator. The $\gamma_{\alpha\beta}$ correlator measures the difference between the correlations projected onto the reaction plane and perpendicular to it. The contributions from correlations in- and out-of-plane can also be evaluated by measuring the charge-dependent two-particle correlator $\delta_{\alpha\beta} \equiv \langle \cos(\varphi_\alpha - \varphi_\beta) \rangle$.

The first experimental results in Au–Au collisions at a centre-of-mass energy per nucleon–nucleon collision $\sqrt{s_{\text{NN}}} = 200$ GeV at the Relativistic Heavy-Ion Collider (RHIC) [27, 28] were compatible with initial expectations for the existence of the CME. The subsequent first measurements at the Large Hadron Collider (LHC) in Pb–Pb collisions at $\sqrt{s_{\text{NN}}} = 2.76$ TeV [29] showed a surprising agreement with the results at lower energies, despite the differences in magnitude of the magnetic field [21–23]. Considering that the charged-particle density, $dN_{\text{ch}}/d\eta$, at the LHC is about three times larger than at RHIC [30, 31], any signal due to CME will be considerably diluted since it is expected to follow a $1/(dN_{\text{ch}}/d\eta)$ scaling [19]. This effect will be referred to as dilution in the following. The similarity of the two measurements was indicative of the existence of background effects, coming mostly from “flowing clusters” – charge-dependent correlations modified by elliptic flow [25]. It was shown in Refs. [32, 33] that the local charge conservation coupled to the anisotropic expansion of the medium could explain most if not all the measurements.

To study background effects, the CMS Collaboration performed measurements of charge-dependent cor-

relations in p–Pb collisions at $\sqrt{s_{\text{NN}}} = 5.02$ TeV [34] and the STAR Collaboration in p–Au and d–Au collisions at $\sqrt{s_{\text{NN}}} = 0.2$ TeV [35]. The results suggest that these correlations are similar to those measured in peripheral Pb–Pb and Au–Au collisions. These results might further indicate the dominance of background effects in peripheral collisions.

These measurements highlighted the need to identify ways of isolating the CME signal from the background. A first attempt was presented by the ALICE Collaboration in Ref. [36] using the Event Shape Engineering method [37]. This method utilises the fluctuations in the shape of the initial state of the system and allows one to select events with the same centrality but different initial geometry, thus varying the background contributions. The study sets an upper limit of 26–33% at 95% confidence level for the CME signal contribution to the charge dependence of $\gamma_{\alpha\beta}$ in the 10–50% centrality interval. A similar study was performed by the CMS Collaboration [38] and the results agree with the measurements in Ref. [36]. A recent study by the ALICE Collaboration [39] found that charge-dependent correlations relative to the higher harmonic symmetry planes can be used as a proxy for the background, assuming that the correlations relative to Ψ_2 and Ψ_3 can be factorised. An upper limit of 15–18% at 95% confidence level for the CME signal has been reported for the 0–40% centrality interval, consistent with previous measurements.

Another approach to address the large backgrounds experimentally is to compare measurements performed in collision systems where the CME contribution is expected to vary significantly, while the background is similar. The STAR Collaboration has recently reported the results of the CME search in an analysis of the three-particle correlator $\gamma_{\alpha\beta}$ measured in collisions of isobar ^{96}Ru – ^{96}Ru and ^{96}Zr – ^{96}Zr nuclei at $\sqrt{s_{\text{NN}}} = 200$ GeV [40]. No anticipated CME signature (i.e., a larger magnitude of $\gamma_{\alpha\beta}$ in Ru–Ru than in Zr–Zr collisions due to a larger magnetic field in the former) was observed in that analysis. However, a quantitative analysis taking into account the small geometrical differences between the isobar nuclei is needed for the interpretation of the measurements. One can also try to separate the CME signal and background by comparing the results from Pb–Pb and Xe–Xe collisions at the LHC since the differences in v_2 are typically within 10% in the 5–70% centrality interval [41] but the magnetic field is expected to be significantly larger in Pb–Pb collisions [42], leading to a similar increase in the CME contribution.

In this article, measurements of charge-dependent azimuthal correlations from Xe–Xe collisions at $\sqrt{s_{\text{NN}}} = 5.44$ TeV are presented. The results are compared with earlier measurements in Pb–Pb collisions at $\sqrt{s_{\text{NN}}} = 5.02$ TeV [39] and calculations from a blast wave parameterisation that incorporate background effects and from the Anomalous Viscous Fluid Dynamics (AVFD) model [43–45]. Furthermore, Monte Carlo (MC) simulations of the magnetic field induced by spectator protons with different initial conditions are used to evaluate the expected change in the CME signal between the Xe–Xe and Pb–Pb collisions. This change is then employed to estimate the fraction of the CME signal in both collision systems.

2 Analysis details

The data set used for these measurements was recorded with the ALICE detector during the 2017 Xe–Xe run at $\sqrt{s_{\text{NN}}} = 5.44$ TeV. A detailed overview of the ALICE detector and its performance are available in Refs. [46, 47]. The Inner Tracking System (ITS) [48], the Time Projection Chamber (TPC) [49], the V0 [50], and the Zero Degree Calorimeter (ZDC) [51], the main subsystems used in this analysis, are briefly described in the following. The ITS and TPC cover the full azimuth within the pseudorapidity range $|\eta| < 0.9$. The ITS consists of six layers of silicon detectors and is employed for tracking, vertex reconstruction, and event selection. The TPC is used to reconstruct charged-particle tracks and to identify particles via specific energy loss, dE/dx . The V0 detector, two arrays of 32 scintillator tiles covering $-3.7 < \eta < -1.7$ (V0C) and $2.8 < \eta < 5.1$ (V0A), is used for triggering, event selection, and the

determination of centrality [52] and symmetry plane Ψ_2 . Both V0 detectors are segmented in four rings in the radial direction with each ring divided into eight sectors in the azimuthal direction. Two tungsten-quartz neutron ZDCs, installed 112.5 meters from the interaction point on each side, are also used for event selection.

The trigger conditions and the event selection criteria can be found in Ref. [53]. Beam-induced background and pileup events are removed using an offline event selection, employing information from the V0, ZDC, and tracking detectors. The primary vertex position is determined from tracks reconstructed in the ITS and TPC as described in Ref. [47]. Approximately 10^6 Xe–Xe events in the 0–70% centrality interval, with a primary vertex position within ± 10 cm from the nominal interaction point along the beam direction, are used in the analysis. The centrality of the collision is estimated from the energy deposition measured in the V0 detector [52].

The charged-particle tracks reconstructed using the ITS and TPC within $|\eta| < 0.8$ and $0.2 \leq p_T < 5.0$ GeV/ c are used to measure the charge-dependent correlations. Each track is required to have a minimum number of 70 space points (out of a maximum of 159) with a χ^2 per TPC space point lower than 4, to cross at least 70 TPC readout rows, and to have the ratio between the number of crossed rows and the number of findable space points in the TPC larger than 0.8. The selected tracks are also required to have at least 2 ITS hits and a χ^2 per ITS hit smaller than 36. In addition, tracks are selected with a distance of closest approach (DCA) to the reconstructed vertex position smaller than 3.2 cm and 2.4 cm in the longitudinal direction (z) and transverse plane (xy), respectively. These selection criteria reduce the contamination from secondary charged particles (i.e., particles originating from weak decays, conversions, and secondary hadronic interactions in the detector material) and fake tracks (random associations of space points) and ensure a track momentum resolution better than 4% in the considered p_T interval [53]. The charged-particle track reconstruction efficiency is estimated from simulations with the HIJING event generator [54, 55] combined with the GEANT3 transport model [56]. These simulations include a detailed description of the detector response. The p_T averaged charge-dependent correlations are corrected for track reconstruction efficiency.

The charge-dependent correlations are measured using two- and three-particle correlators expressed as

$$\begin{aligned} \delta_{\alpha\beta} &\equiv \langle \cos(\varphi_\alpha - \varphi_\beta) \rangle = \langle \cos(\Delta\varphi_\alpha) \cos(\Delta\varphi_\beta) \rangle + \langle \sin(\Delta\varphi_\alpha) \sin(\Delta\varphi_\beta) \rangle \\ &= \langle v_{1,\alpha} v_{1,\beta} \rangle + B_{\text{in}} + \langle a_{1,\alpha} a_{2,\beta} \rangle + B_{\text{out}}, \end{aligned} \quad (2)$$

$$\begin{aligned} \gamma_{\alpha\beta} &\equiv \langle \cos(\varphi_\alpha + \varphi_\beta - 2\Psi_2) \rangle = \langle \cos(\Delta\varphi_\alpha) \cos(\Delta\varphi_\beta) \rangle - \langle \sin(\Delta\varphi_\alpha) \sin(\Delta\varphi_\beta) \rangle \\ &= \langle v_{1,\alpha} v_{1,\beta} \rangle + B_{\text{in}} - \langle a_{1,\alpha} a_{2,\beta} \rangle - B_{\text{out}}, \end{aligned} \quad (3)$$

where $\Delta\varphi_{\alpha(\beta)} = \varphi_{\alpha(\beta)} - \Psi_2$, and B_{in} and B_{out} denote background contributions projected onto Ψ_2 and perpendicular to it, respectively. The term $\langle v_{1,\alpha} v_{1,\beta} \rangle$ is expected to have negligible charge dependence at midrapidity [57]. In addition, $\langle v_1 \rangle$ at midrapidity is zero for a symmetric collision. While $\gamma_{\alpha\beta}$ suppresses background contributions at the level of v_2 (i.e., the relative difference between the particle production in-plane and out-of-plane), $\delta_{\alpha\beta}$ is dominated by short-range correlations unrelated to Ψ_2 (“non-flow”), such as inter-jet correlations and resonance decays.

The orientation of the symmetry plane Ψ_2 is estimated from the azimuthal distribution of the energy deposition measured by the V0A detector, with the x and y components given by

$$Q_{2,x} = \sum_j w_j \cos(2\varphi_j), \quad Q_{2,y} = \sum_j w_j \sin(2\varphi_j), \quad (4)$$

where the index j runs over the 32 sectors of the V0A detector, φ_j is the azimuthal angle of sector j defined by the geometric centre, and w_j is the amplitude of the measured signal in that sector. The symmetry plane resolution is calculated from correlations between the symmetry planes determined with the TPC, the V0A, and the V0C detectors [26]. The effect of the decorrelation of Ψ_2 between mid and

Table 1: Summary of absolute systematic uncertainties on the charge-dependent correlations. The uncertainties depend on centrality, whose minimum and maximum values are listed here.

	Opposite charge	Same charge
$\delta_{\alpha\beta}$	$(6.8 - 33) \times 10^{-5}$	$(3.8 - 13) \times 10^{-5}$
$\gamma_{\alpha\beta}$	$(1.0 - 8.3) \times 10^{-5}$	$(1.4 - 5.9) \times 10^{-5}$

forward pseudorapidity has been estimated to be less than 3% for v_2 [58]. Any non-uniform detector response is taken into account by adjusting the components of the \mathbf{Q}_2 vector using a recentering procedure (i.e., subtraction of the \mathbf{Q}_2 vector averaged over many events from the \mathbf{Q}_2 vector of each event) [59]. The non-flow contributions to the charge-dependent azimuthal correlations are greatly suppressed by the large pseudorapidity separation between the TPC and the VOA ($|\Delta\eta| > 2.0$).

The absolute systematic uncertainties were estimated from the variation of the results with different event and track-selection criteria. The event selection contributions were determined by varying the range of the reconstructed collision vertex position from the nominal interaction point along the beam direction, estimating centrality from the number of hits in the first or second layer of the ITS, and imposing stricter pileup rejection criteria than the default selection. Systematic uncertainties related to track selection criteria were evaluated by changing the ITS hit requirements, varying the minimum number of TPC space points, changing the minimum number of crossed TPC readout rows and the ratio between the number of crossed rows and the number of findable space points in the TPC, rejecting tracks close to the TPC sector boundaries to which the sensitive readout rows do not extend, and comparing any differences between results with only positive and only negative charges for pairs of particles with same charge. Finally, changes of the results due to uncertainties in the tracking efficiency arising from an imperfect description in the simulation of the relative abundances of different particle species and their different reconstruction efficiencies [60] were considered as part of the systematic uncertainties. The largest contribution to the systematic uncertainties for $\gamma_{\alpha\beta}$ and $\delta_{\alpha\beta}$ is given by the centrality estimation and track-selection criteria, respectively. The systematic uncertainties are evaluated for each centrality interval. The different sources are assumed uncorrelated and are added in quadrature as an estimate of the total systematic uncertainties if their deviations from the nominal values are significant according to the Barlow criterion [61]. The resulting systematic uncertainties increase from central to peripheral collisions and are summarised in Table 1.

3 Results

Figure 1 compares the $\delta_{\alpha\beta}$ and $\gamma_{\alpha\beta}$ correlators for same- and opposite-charge pairs in Xe–Xe collisions at $\sqrt{s_{\text{NN}}} = 5.44$ TeV to those measured in Pb–Pb collisions at $\sqrt{s_{\text{NN}}} = 5.02$ TeV [39] as a function of centrality and average charged-particle multiplicity density $\langle dN_{\text{ch}}/d\eta \rangle$ at midrapidity [62, 63]. The results for same-charge pairs denote the average between pairs of particles with only positive and only negative charges since the two combinations are consistent within statistical uncertainties. Both correlators exhibit strong dependence on the charge-sign combination and qualitatively similar centrality dependence in the two systems. For $\delta_{\alpha\beta}$, the magnitude of the same- and opposite-charge pair correlations is positive and increases from central to peripheral collisions. In contrast to the CME expectation, the correlation for the opposite-charge pairs is stronger than for the same-charge combinations, indicating that background dominates these measurements. For $\gamma_{\alpha\beta}$, the magnitude of opposite-charge pair correlations is close to zero within uncertainties for most of the centrality intervals, while it decreases from central to peripheral collisions becoming more negative for same-charge pairs. Thus, the correlation of opposite-charge pairs is weaker than for same-charge pairs. This ordering is compatible with a charge separation with respect to the reaction plane expected in the presence of the CME.

The $\delta_{\alpha\beta}$ for same-charge pairs shows small (if any) differences between Xe–Xe and Pb–Pb collisions within uncertainties, while the correlations for opposite-charge pairs have larger magnitude in Xe–Xe

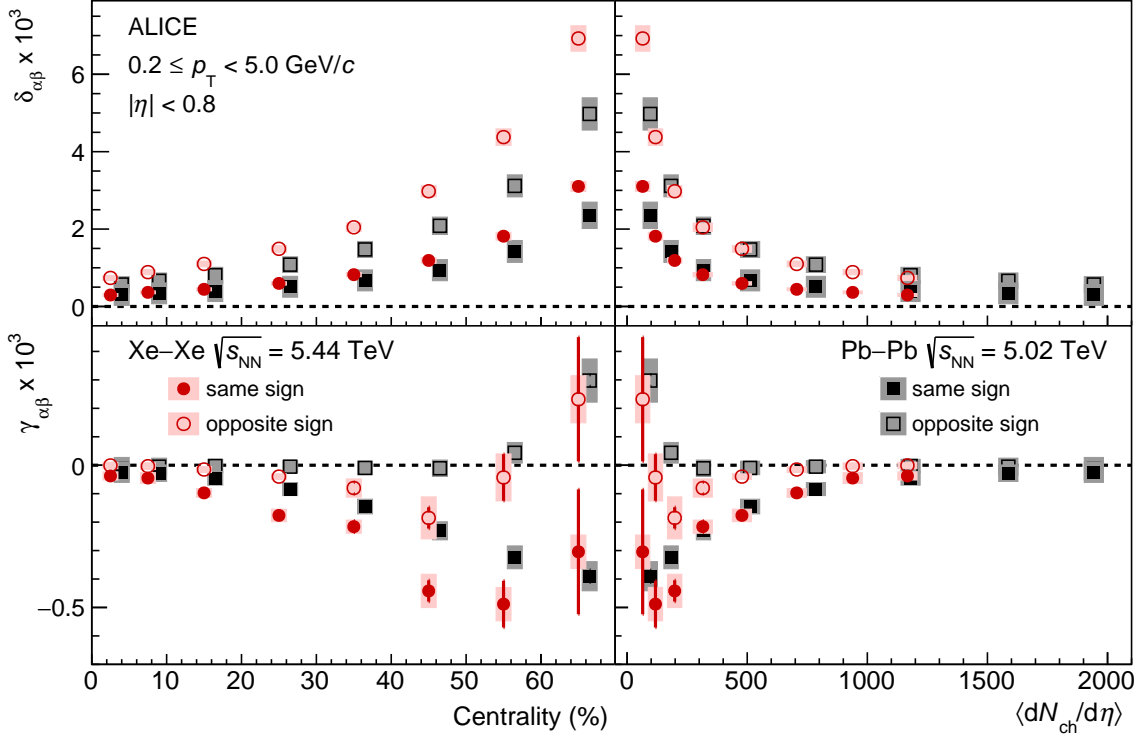


Figure 1: The $\delta_{\alpha\beta}$ (top panels) and $\gamma_{\alpha\beta}$ (bottom panels) correlators as a function of centrality (left panels) and charged-particle density [62, 63] (right panels) for pairs of particles with same (closed markers) and opposite (open markers) charges from Xe–Xe collisions at $\sqrt{s_{NN}} = 5.44$ TeV (red circles) compared to Pb–Pb collisions at $\sqrt{s_{NN}} = 5.02$ TeV (black squares) [39]. The Pb–Pb points are slightly shifted along the horizontal axis for better visibility in the left panels. Bars (boxes) denote statistical (systematic) uncertainties.

collisions in the 10–70% centrality interval. The $\gamma_{\alpha\beta}$ for same- and opposite-charge pairs from Xe–Xe and Pb–Pb collisions have similar magnitudes within uncertainties in the 0–10% and 50–70% centrality ranges, while the correlations are stronger in Xe–Xe collisions in the 10–50% centrality interval. These observations can be attributed to the different number of particles produced in the collision within a given centrality interval between the two systems that dilutes the correlations. This is supported by the fact that the $\delta_{\alpha\beta}$ and $\gamma_{\alpha\beta}$ for same- and opposite-charge pairs from Xe–Xe collisions are consistent within uncertainties with the corresponding Pb–Pb results when reported as a function of $\langle dN_{ch}/d\eta \rangle$.

The $\gamma_{\alpha\beta}$ correlator is also investigated as a function of the pseudorapidity difference $\Delta\eta = |\eta_\alpha - \eta_\beta|$, the transverse momentum difference $\Delta p_T = |p_{T\alpha} - p_{T\beta}|$, and the average transverse momentum $\langle p_T \rangle = (p_{T\alpha} + p_{T\beta})/2$ of the pair. Figure 2 presents these results for same- and opposite-charge pairs in the 20–30% centrality interval compared to measurements performed in 30–40% Pb–Pb collisions [39]. Different Xe–Xe and Pb–Pb centrality intervals are selected since they have similar transverse densities ($1/S dN_{ch}/d\eta \sim 10 \text{ fm}^{-2}$ with S being the transverse area) and transverse sizes ($R = \sqrt{S/\pi} \sim 4 \text{ fm}$) [41], thus the contribution from dilution effects is comparable. In addition, the value of v_2/ε_2 (ε_2 is the second-order eccentricity coefficient and characterises the elliptic shape of the initial geometry) and the influence of radial flow are similar in the two systems for these centrality classes [41, 53]. The opposite-charge pair correlations from Xe–Xe collisions show a weak dependence on $\Delta\eta$ and $\langle p_T \rangle$, while they increase with increasing Δp_T of the pair. The correlations for the same-charge pairs do not exhibit any significant dependence on Δp_T and $\langle p_T \rangle$ within uncertainties. These correlations show a strong dependence on $\Delta\eta$ with a width of approximately one unit in pseudorapidity difference. The Xe–Xe and

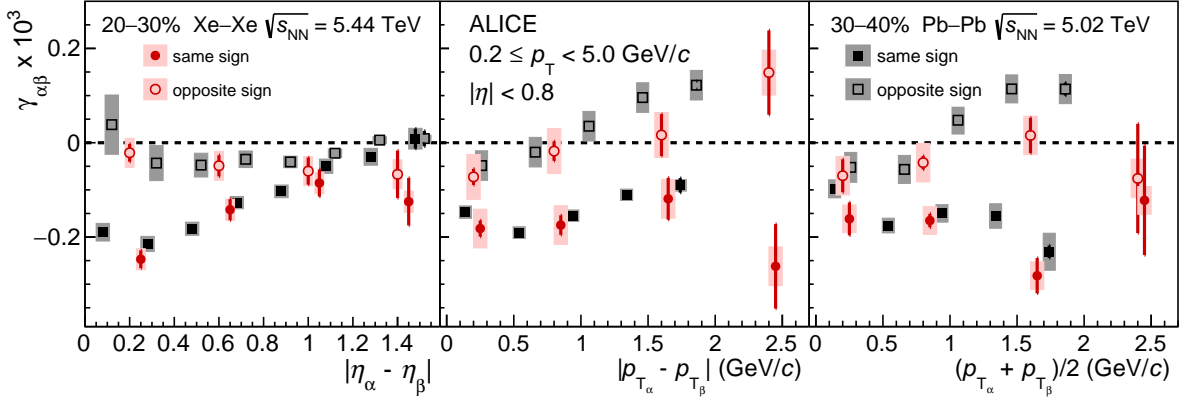


Figure 2: The dependence of $\gamma_{\alpha\beta}$ on the pseudorapidity difference $|\eta_\alpha - \eta_\beta|$ (left panel), the transverse momentum difference $|p_{T_\alpha} - p_{T_\beta}|$ (middle panel), and the average transverse momentum $(p_{T_\alpha} + p_{T_\beta})/2$ (right panel) for pairs of particles with same (closed markers) and opposite (open markers) charges from 20–30% Xe–Xe collisions at $\sqrt{s_{NN}} = 5.44$ TeV (red circles) compared to results from 30–40% Pb–Pb collisions at $\sqrt{s_{NN}} = 5.02$ TeV (black squares) [39]. The Pb–Pb and Xe–Xe same-charge points are slightly shifted along the horizontal axis for better visibility in all panels. Bars (boxes) denote statistical (systematic) uncertainties.

Pb–Pb results are compatible within uncertainties demonstrating similar behaviour of this observable despite the differences in the magnetic field.

To get insight into the origin of the charge-dependent effects observed in Xe–Xe collisions, two different approaches were investigated. The first one relies on a blast wave (BW) model based on a parameterisation from Ref. [64]. Input parameters of the model are tuned to describe the p_T spectra [65] and the p_T -differential v_2 values [66] of charged pions and kaons, as well as of protons and antiprotons, measured in the same collision system and centre-of-mass energy. To account for the main source of background in the measurements reported in this article, the model was further extended by including effects from local charge conservation (LCC). This was done by generating sources uniformly at the surface of the ellipse that surrounds the centre of the system and allowing them to decay into particles with opposite charge. In this extension of the BW model, the number of sources that emit oppositely-charged pairs is tuned separately for each centrality interval to reproduce the centrality dependence of $\Delta\delta_{\alpha\beta} \equiv \delta_{\alpha\beta}^{\text{opp.}} - \delta_{\alpha\beta}^{\text{same}}$, the correlator that is mainly sensitive to background effects. This is illustrated in the upper panel of Fig. 3, where the BW curve is represented by the blue, solid line that goes through the experimental data points. The tuned model is then used to extract the expectation for the centrality dependence of $\Delta\gamma_{\alpha\beta} \equiv \gamma_{\alpha\beta}^{\text{opp.}} - \gamma_{\alpha\beta}^{\text{same}}$, shown in the lower panel of Fig. 3. The width of the band reflects the uncertainty obtained by propagating the corresponding uncertainties of the model parameters using a sub-sampling method. It can be seen that the BW model describes fairly well the measured data points for all centrality intervals. This is in contrast to the picture that emerged in Pb–Pb collisions, where following a similar procedure the same model underestimated the measurements of $\Delta\gamma_{\alpha\beta}$ by as much as $\approx 40\%$ [39].

Additional insight can be obtained by comparing the results with calculations from the Anomalous Viscous Fluid Dynamics (AVFD) model [43–45]. It relies on a Glauber model description of the initial state of the collision and accounts for the development of the early-stage electromagnetic fields as well as for the propagation of anomalous fermion currents. The expanding medium is described using a 2+1 dimensional viscous hydrodynamics (VISH2+1) code [67] which is coupled to a hadron cascade model (UrQMD) [68, 69]. Within AVFD, the final-state CME signal induced by the initial chirality imbalance is controlled by the axial current density n_5/s . At the same time, the relevant background in AVFD is governed by the amount of positive and negative charged partners emitted from the same fluid element

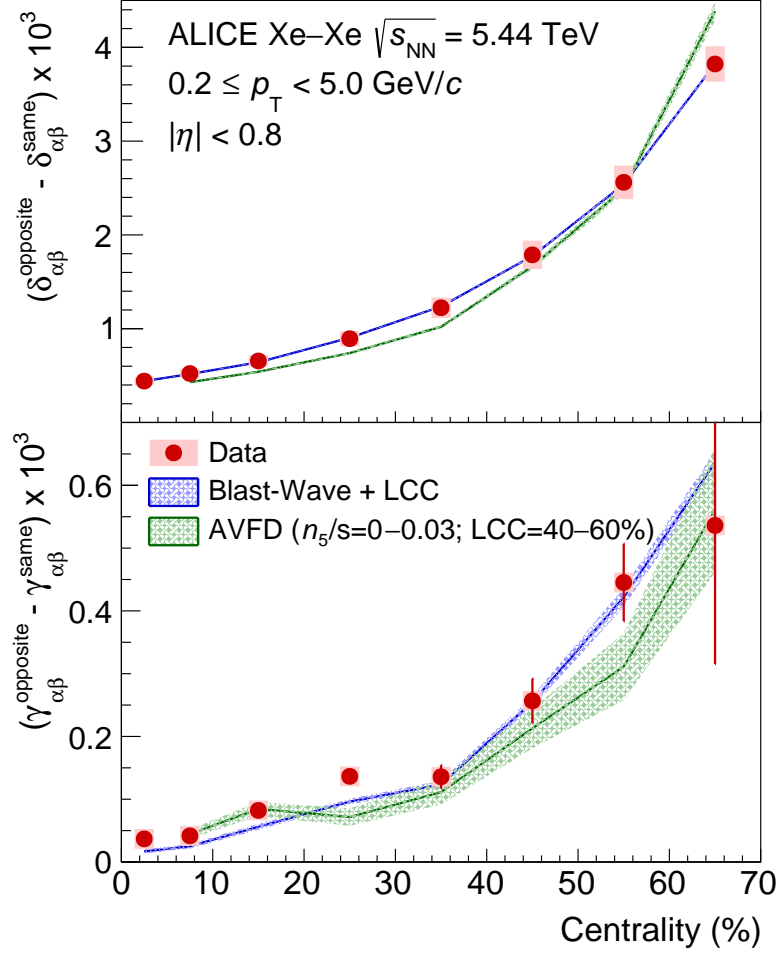


Figure 3: Centrality evolution of the difference between same- and opposite-charge pair correlations for $\delta_{\alpha\beta}$ (top panel) and $\gamma_{\alpha\beta}$ (bottom panel) compared to model calculations: blast wave (BW) parameterisation [64] coupled to local charge conservation (LCC) effects (blue curves) and Anomalous Viscous Fluid Dynamics (AVFD) [43, 44] (green curves). The BW+LCC model is tuned to reproduce the centrality dependence of $\Delta\delta_{\alpha\beta}$, while AVFD is tuned to describe simultaneously the centrality dependence of $\Delta\delta_{\alpha\beta}$ and $\Delta\gamma_{\alpha\beta}$. Bars (boxes) denote statistical (systematic) uncertainties on the data points, while the thickness of the curves represents the uncertainties on the model calculations.

relative to the total multiplicity of the event, i.e., the LCC percentage. The model was first calibrated to describe the centrality dependence of both the charged-particle density [63] and the elliptic flow [41]. As a second step, the dependence of $\Delta\delta_{\alpha\beta}$ and $\Delta\gamma_{\alpha\beta}$ on both the CME signal and the background was determined, by analysing samples with either increasing values of n_5/s or LCC percentage, respectively [42]. These results made it possible to extract the combination of n_5/s and LCC percentage that describes the data and led to a quantitative simultaneous description of the centrality dependence of $\Delta\delta_{\alpha\beta}$ and $\Delta\gamma_{\alpha\beta}$ [42]. This is illustrated in the two panels of Fig. 3. Also in this case, the width of the band reflects the uncertainty obtained by propagating the corresponding uncertainties of the model parameters using a sub-sampling method. The experimental data points can be described by large values of LCC contribution, between 40% and 60% for peripheral and more central Xe–Xe collisions, respectively. In addition, the values of n_5/s extracted from this procedure did not exhibit any significant centrality dependence and were compatible with zero within uncertainties [42]. Similar to the conclusion extracted from the BW

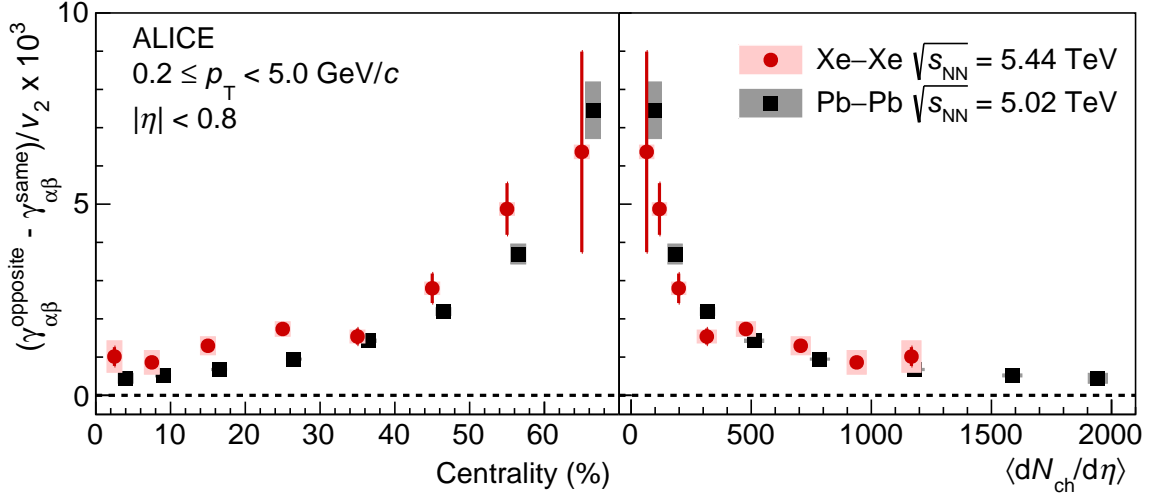


Figure 4: Difference between opposite- and same-charge pair correlations for $\gamma_{\alpha\beta}$ divided by v_2 [41] as a function of centrality (left) and charged-particle density (right) compared to results from Pb–Pb collisions at $\sqrt{s_{NN}} = 5.02$ TeV [39]. The Pb–Pb points are slightly shifted along the horizontal axis for better visibility in the left panel. Bars (boxes) denote statistical (systematic) uncertainties.

model, the study within the AVFD framework indicates that the experimental measurements in Xe–Xe collisions are dominated by background.

The charge separation effect can be further studied using the difference between opposite- and same-charge pair correlations $\Delta\gamma_{\alpha\beta}$ and the CME signal expectations from MC calculations employed as guidance. A comparison between $\Delta\gamma_{\alpha\beta}$ divided by v_2 [41] in Xe–Xe collisions and that measured in Pb–Pb collisions [39] is presented as a function of centrality and charged-particle density [62, 63] in Fig. 4. The value of $\Delta\gamma_{\alpha\beta}/v_2$ is positive for all centralities and its magnitude increases from central to peripheral collisions. Furthermore, it is slightly higher in Xe–Xe than Pb–Pb collisions in the 10–60% centrality interval. However, the Xe–Xe and Pb–Pb data points fall approximately onto the same curve when reported as a function of $\langle dN_{ch}/d\eta \rangle$.

The expected centrality dependence of the CME signal in Xe–Xe and Pb–Pb collisions is estimated from MC Glauber [70] simulations including a magnetic field [36]. In these calculations, the ^{208}Pb nucleus is spherical while the ^{129}Xe nucleus is deformed with a deformation parameter $\beta_2 = 0.18 \pm 0.02$ [52]. The centrality classes are determined from the multiplicity of charged particles in the acceptance of the V0 detector, which is generated according to a negative binomial distribution with parameters taken from Ref. [71]. The magnetic field is calculated at the origin from the number of spectator protons using Eq. (A.6) from Ref. [19] with the proper time $\tau = 0.1$ fm/c. Figure 5 shows the centrality dependence of $\langle (eB)^2 \cos(2(\Psi_B - \Psi_2)) \rangle$ (Ψ_B is the direction of the magnetic field \vec{B}), which is the expected CME signal contribution in $\gamma_{\alpha\beta}$, for the two collision systems. The expected CME signal is stronger in Pb–Pb than Xe–Xe collisions in a given centrality interval due to the smaller magnetic field strength and a larger decorrelation between Ψ_B and Ψ_2 in Xe–Xe collisions. Similar results are found using T_RENTo [72] initial conditions. This observation coupled to the agreement of $\Delta\gamma_{\alpha\beta}$ between the two collision systems (see Fig. 4) points to a large background contribution to $\gamma_{\alpha\beta}$ in Xe–Xe collisions.

The large differences in the CME signal expectations and the small variations in v_2 ($< 10\%$ for the 5–70% centrality interval) [41] between the two collision systems can be used to disentangle the potential CME signal from the background in Xe–Xe and Pb–Pb collisions. Assuming that both the CME signal

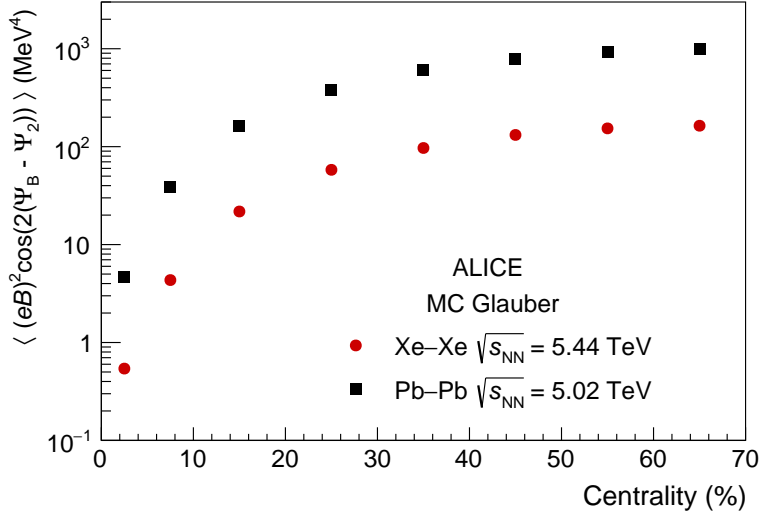


Figure 5: The expected CME signal as a function of centrality from MC Glauber simulations for Xe–Xe and Pb–Pb collisions [70] (see text for details).

and the background scale with $dN_{\text{ch}}/d\eta$, the charge dependence of $\gamma_{\alpha\beta}$ for the two collision systems can be expressed using a two-component approach similar to the one proposed in Ref. [73]

$$\Gamma^{\text{Xe–Xe}} = sB^{\text{Xe–Xe}} + bv_2^{\text{Xe–Xe}}, \quad (5)$$

$$\Gamma^{\text{Pb–Pb}} = sB^{\text{Pb–Pb}} + bv_2^{\text{Pb–Pb}}, \quad (6)$$

where $\Gamma \equiv \gamma_{\alpha\beta} dN_{\text{ch}}/d\eta$, $B \equiv \langle (eB)^2 \cos(2(\Psi_B - \Psi_2)) \rangle$, and v_2 is taken from Ref. [41] and $\gamma_{\alpha\beta}^{\text{Pb–Pb}}$ from Ref. [39]. The s and b parameters quantify the signal and background contributions, respectively, and do not depend on collision system as a result of the assumption that both scale with $dN_{\text{ch}}/d\eta$. While this scaling is expected for b since it is dominated by flowing clusters [25], the domains responsible for s are small and thus they can be considered as “usual” clusters which scale with $dN_{\text{ch}}/d\eta$. These parameters can be used to calculate the fractions of the CME signal (denoted as f_{CME}) in Xe–Xe and Pb–Pb collisions as

$$f_{\text{CME}} = \frac{sB}{sB + bv_2}. \quad (7)$$

The smaller CME signal in Xe–Xe collisions also results in a tighter limit on f_{CME} in Xe–Xe than in Pb–Pb collisions. It is worth noting that the CME fractions in the two collision systems are correlated because both are calculated with the same s and b parameters, extracted from the data using Eqs. 5 and 6.

Figure 6 presents the centrality dependence of f_{CME} in Xe–Xe and Pb–Pb collisions for the two models used in this study. The uncertainties in the CME fractions are obtained adding in quadrature the statistical and systematic uncertainties in Eqs. 5 and 6. The f_{CME} does not depend significantly on the proper time used to calculate the magnetic field since varying the value from 0.1 fm/c to 0.01 fm/c, 0.5 fm/c, and 1 fm/c yields similar CME fractions. The f_{CME} is compatible with zero up to 30% centrality in both systems and then becomes positive for midcentral and peripheral collisions with larger values in Pb–Pb than in Xe–Xe. The CME fraction for the 0–30% centrality interval in Pb–Pb collisions agrees with the one reported in Ref. [39]. Fitting the data points in the centrality range 0–70% with a constant function neglecting any centrality dependence gives $f_{\text{CME}} = -0.003 \pm 0.010$ ($f_{\text{CME}} = -0.001 \pm 0.012$) and $f_{\text{CME}} = 0.147 \pm 0.061$ ($f_{\text{CME}} = 0.150 \pm 0.062$) for MC Glauber (T_RENTO) initial conditions in Xe–Xe and Pb–Pb collisions, respectively. These results are consistent with zero CME fraction in Xe–Xe

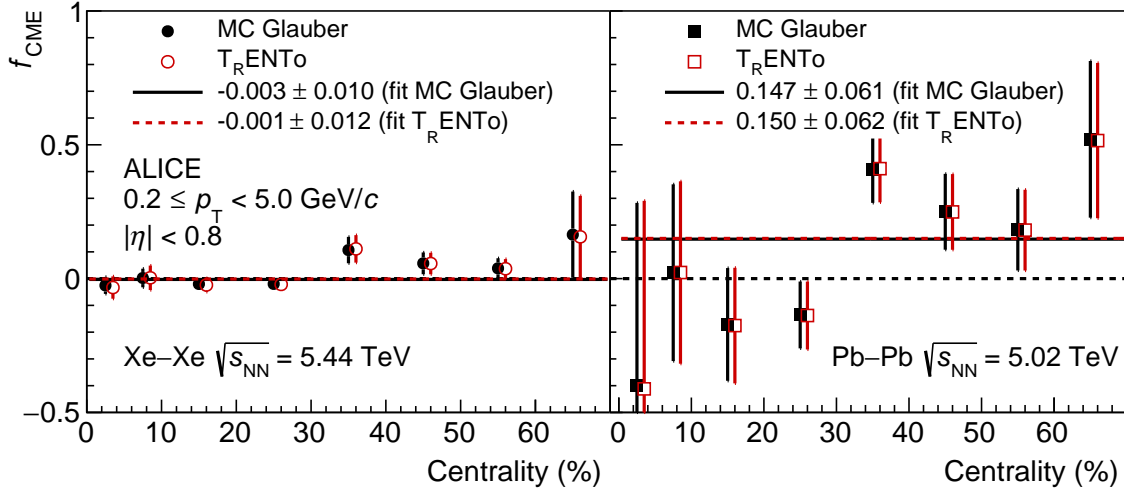


Figure 6: Centrality dependence of the CME fraction extracted using Eq. 7 with the expected CME signal from MC Glauber [70] (closed markers) and $T_{R\text{ENTo}}$ [72] (open markers) models (see text for details). The $T_{R\text{ENTo}}$ points are slightly shifted along the horizontal axis for better visibility.

collisions and correspond to upper limits on f_{CME} of 2% (3%) and 25% (32%) at 95% (99.7%) confidence level for the 0–70% centrality interval in Xe–Xe and Pb–Pb collisions, respectively. The limits are estimated assuming Gaussian uncertainties.

4 Summary

The charge-dependent two- and three-particle correlators $\delta_{\alpha\beta}$ and $\gamma_{\alpha\beta}$ have been measured in Xe–Xe collisions at $\sqrt{s_{\text{NN}}} = 5.44$ TeV. The charge dependence of these correlators is strongly correlated with centrality, increasing from central to peripheral collisions, and is qualitatively similar to those reported in Pb–Pb collisions. The difference between the Xe–Xe and Pb–Pb results mostly arises from dilution effects since the data points from both collision systems fall approximately onto the same curve when presented as a function of charged-particle density. Monte Carlo simulations with different initial state models predict a significantly larger magnitude of the CME signal in Pb–Pb than Xe–Xe collisions, which implies that the dominant contribution to $\gamma_{\alpha\beta}$ in Xe–Xe collisions is due to background effects. The magnitude of the charge dependence of $\gamma_{\alpha\beta}$ is described over the entire centrality range by a blast wave parameterisation that incorporates local charge conservation tuned to reproduce the components of the background. This magnitude is also reproduced by Anomalous Viscous Fluid Dynamics calculations with large contributions from local charge conservation effects and values of the CME signal close to zero, thus indicating that the background is the dominant contribution to the three-particle correlator. In order to get a quantitative estimate of the signal and background contributions, the measured values of $\gamma_{\alpha\beta}$ in Xe–Xe and Pb–Pb collisions are compared using a two-component approach. This procedure allows one to estimate the fraction of the CME signal in both collision systems. Averaging over the 0–70% centrality interval, an upper limit of 2% (3%) and 25% (32%) is estimated at 95% (99.7%) confidence level for the CME contribution to the charge dependence of $\gamma_{\alpha\beta}$ in Xe–Xe and Pb–Pb collisions, respectively.

References

- [1] F. Karsch and E. Laermann, “Thermodynamics and in medium hadron properties from lattice QCD”, *World Scientific* (2004) 1–59, arXiv:hep-lat/0305025.
- [2] F. Karsch, E. Laermann, and A. Peikert, “Quark mass and flavor dependence of the QCD phase transition”, *Nucl. Phys. B* **605** (2001) 579–599, arXiv:hep-lat/0012023.
- [3] F. Karsch, E. Laermann, and A. Peikert, “The Pressure in two flavor, (2+1)-flavor and three flavor QCD”, *Phys. Lett. B* **478** (2000) 447–455, arXiv:hep-lat/0002003.
- [4] F. Karsch, “Lattice results on QCD thermodynamics”, *Nucl. Phys. A* **698** (2002) 199–208, arXiv:hep-ph/0103314.
- [5] C. R. Allton *et al.*, “The QCD thermal phase transition in the presence of a small chemical potential”, *Phys. Rev. D* **66** (2002) 074507, arXiv:hep-lat/0204010.
- [6] A. Bazavov *et al.*, “Equation of state and QCD transition at finite temperature”, *Phys. Rev. D* **80** (2009) 014504, arXiv:0903.4379 [hep-lat].
- [7] A. Bazavov *et al.*, “The chiral and deconfinement aspects of the QCD transition”, *Phys. Rev. D* **85** (2012) 054503, arXiv:1111.1710 [hep-lat].
- [8] S. Borsanyi *et al.*, “The QCD equation of state with dynamical quarks”, *JHEP* **11** (2010) 077, arXiv:1007.2580 [hep-lat].
- [9] CMS Collaboration, S. Chatrchyan *et al.*, “Measurement of the pseudorapidity and centrality dependence of the transverse energy density in PbPb collisions at $\sqrt{s_{\text{NN}}} = 2.76$ TeV”, *Phys. Rev. Lett.* **109** (2012) 152303, arXiv:1205.2488 [nucl-ex].
- [10] ALICE Collaboration, J. Adam *et al.*, “Direct photon production in Pb–Pb collisions at $\sqrt{s_{\text{NN}}} = 2.76$ TeV”, *Phys. Lett. B* **754** (2016) 235–248, arXiv:1509.07324 [nucl-ex].
- [11] ALICE Collaboration, J. Adam *et al.*, “Measurement of transverse energy at midrapidity in Pb–Pb collisions at $\sqrt{s_{\text{NN}}} = 2.76$ TeV”, *Phys. Rev. C* **94** no. 3, (2016) 034903, arXiv:1603.04775 [nucl-ex].
- [12] T. Lee, “A Theory of Spontaneous T Violation”, *Phys. Rev. D* **8** (1973) 1226–1239.
- [13] T. Lee and G. Wick, “Vacuum Stability and Vacuum Excitation in a Spin 0 Field Theory”, *Phys. Rev. D* **9** (1974) 2291–2316.
- [14] P. Morley and I. Schmidt, “Strong P, CP, T Violations in Heavy Ion Collisions”, *Z. Phys. C* **26** (1985) 627.
- [15] D. Kharzeev, R. Pisarski, and M. H. Tytgat, “Possibility of spontaneous parity violation in hot QCD”, *Phys. Rev. Lett.* **81** (1998) 512–515, arXiv:hep-ph/9804221.
- [16] D. Kharzeev and R. D. Pisarski, “Pionic measures of parity and CP violation in high-energy nuclear collisions”, *Phys. Rev. D* **61** (2000) 111901, arXiv:hep-ph/9906401.
- [17] D. E. Kharzeev, “Topology, magnetic field, and strongly interacting matter”, *Ann. Rev. Nucl. Part. Sci.* **65** (2015) 193–214, arXiv:1501.01336 [hep-ph].
- [18] D. Kharzeev and A. Zhitnitsky, “Charge separation induced by P-odd bubbles in QCD matter”, *Nucl. Phys. A* **797** (2007) 67–79, arXiv:0706.1026 [hep-ph].

- [19] D. E. Kharzeev, L. D. McLerran, and H. J. Warringa, “The Effects of topological charge change in heavy ion collisions: ‘Event by event P and CP violation’”, *Nucl. Phys. A* **803** (2008) 227–253, arXiv:0711.0950 [hep-ph].
- [20] K. Fukushima, D. E. Kharzeev, and H. J. Warringa, “The Chiral Magnetic Effect”, *Phys. Rev. D* **78** (2008) 074033, arXiv:0808.3382 [hep-ph].
- [21] V. Skokov, A. Illarionov, and V. Toneev, “Estimate of the magnetic field strength in heavy-ion collisions”, *Int. J. Mod. Phys. A* **24** (2009) 5925–5932, arXiv:0907.1396 [nucl-th].
- [22] A. Bzdak and V. Skokov, “Event-by-event fluctuations of magnetic and electric fields in heavy ion collisions”, *Phys. Lett. B* **710** (2012) 171–174, arXiv:1111.1949 [hep-ph].
- [23] W.-T. Deng and X.-G. Huang, “Event-by-event generation of electromagnetic fields in heavy-ion collisions”, *Phys. Rev. C* **85** (2012) 044907, arXiv:1201.5108 [nucl-th].
- [24] S. Voloshin and Y. Zhang, “Flow study in relativistic nuclear collisions by Fourier expansion of Azimuthal particle distributions”, *Z. Phys.* **C70** (1996) 665–672, arXiv:hep-ph/9407282.
- [25] S. A. Voloshin, “Parity violation in hot QCD: How to detect it”, *Phys. Rev.* **C70** (2004) 057901, arXiv:hep-ph/0406311.
- [26] A. M. Poskanzer and S. A. Voloshin, “Methods for analyzing anisotropic flow in relativistic nuclear collisions”, *Phys. Rev.* **C58** (1998) 1671–1678, arXiv:nucl-ex/9805001.
- [27] **STAR** Collaboration, B. I. Abelev *et al.*, “Azimuthal Charged-Particle Correlations and Possible Local Strong Parity Violation”, *Phys. Rev. Lett.* **103** (2009) 251601, arXiv:0909.1739 [nucl-ex].
- [28] **STAR** Collaboration, B. I. Abelev *et al.*, “Observation of charge-dependent azimuthal correlations and possible local strong parity violation in heavy ion collisions”, *Phys. Rev. C* **81** (2010) 054908, arXiv:0909.1717 [nucl-ex].
- [29] **ALICE** Collaboration, B. Abelev *et al.*, “Charge separation relative to the reaction plane in Pb–Pb collisions at $\sqrt{s_{NN}} = 2.76$ TeV”, *Phys. Rev. Lett.* **110** no. 1, (2013) 012301, arXiv:1207.0900 [nucl-ex].
- [30] **ALICE** Collaboration, K. Aamodt *et al.*, “Charged-particle multiplicity density at mid-rapidity in central Pb–Pb collisions at $\sqrt{s_{NN}} = 2.76$ TeV”, *Phys. Rev. Lett.* **105** (2010) 252301, arXiv:1011.3916 [nucl-ex].
- [31] **ALICE** Collaboration, K. Aamodt *et al.*, “Centrality dependence of the charged-particle multiplicity density at mid-rapidity in Pb–Pb collisions at $\sqrt{s_{NN}} = 2.76$ TeV”, *Phys. Rev. Lett.* **106** (2011) 032301, arXiv:1012.1657 [nucl-ex].
- [32] S. Schlichting and S. Pratt, “Charge conservation at energies available at the BNL Relativistic Heavy Ion Collider and contributions to local parity violation observables”, *Phys. Rev. C* **83** (2011) 014913, arXiv:1009.4283 [nucl-th].
- [33] S. Pratt, S. Schlichting, and S. Gavin, “Effects of Momentum Conservation and Flow on Angular Correlations at RHIC”, *Phys. Rev. C* **84** (2011) 024909, arXiv:1011.6053 [nucl-th].
- [34] **CMS** Collaboration, V. Khachatryan *et al.*, “Observation of charge-dependent azimuthal correlations in p -Pb collisions and its implication for the search for the chiral magnetic effect”, *Phys. Rev. Lett.* **118** no. 12, (2017) 122301, arXiv:1610.00263 [nucl-ex].

- [35] **STAR** Collaboration, J. Adam *et al.*, “Charge-dependent pair correlations relative to a third particle in $p + \text{Au}$ and $d + \text{Au}$ collisions at RHIC”, *Phys. Lett. B* **798** (2019) 134975, arXiv:1906.03373 [nucl-ex].
- [36] **ALICE** Collaboration, S. Acharya *et al.*, “Constraining the magnitude of the Chiral Magnetic Effect with Event Shape Engineering in Pb–Pb collisions at $\sqrt{s_{\text{NN}}} = 2.76 \text{ TeV}$ ”, *Phys. Lett.* **B777** (2018) 151–162, arXiv:1709.04723 [nucl-ex].
- [37] J. Schukraft, A. Timmins, and S. A. Voloshin, “Ultra-relativistic nuclear collisions: event shape engineering”, *Phys. Lett.* **B719** (2013) 394–398, arXiv:1208.4563 [nucl-ex].
- [38] **CMS** Collaboration, A. M. Sirunyan *et al.*, “Constraints on the chiral magnetic effect using charge-dependent azimuthal correlations in $p\text{Pb}$ and PbPb collisions at the CERN Large Hadron Collider”, *Phys. Rev. C* **97** no. 4, (2018) 044912, arXiv:1708.01602 [nucl-ex].
- [39] **ALICE** Collaboration, S. Acharya *et al.*, “Constraining the Chiral Magnetic Effect with charge-dependent azimuthal correlations in Pb–Pb collisions at $\sqrt{s_{\text{NN}}} = 2.76$ and 5.02 TeV ”, *JHEP* **09** (2020) 160, arXiv:2005.14640 [nucl-ex].
- [40] **STAR** Collaboration, M. Abdallah *et al.*, “Search for the chiral magnetic effect with isobar collisions at $\sqrt{s_{\text{NN}}}=200 \text{ GeV}$ by the STAR Collaboration at the BNL Relativistic Heavy Ion Collider”, *Phys. Rev. C* **105** no. 1, (2022) 014901, arXiv:2109.00131 [nucl-ex].
- [41] **ALICE** Collaboration, S. Acharya *et al.*, “Anisotropic flow in Xe–Xe collisions at $\sqrt{s_{\text{NN}}} = 5.44 \text{ TeV}$ ”, *Phys. Lett. B* **784** (2018) 82–95, arXiv:1805.01832 [nucl-ex].
- [42] P. Christakoglou, S. Qiu, and J. Staa, “Systematic study of the chiral magnetic effect with the AVFD model at LHC energies”, *Eur. Phys. J. C* **81** no. 8, (2021) 717, arXiv:2106.03537 [nucl-th].
- [43] S. Shi, Y. Jiang, E. Lilleskov, and J. Liao, “Anomalous Chiral Transport in Heavy Ion Collisions from Anomalous-Viscous Fluid Dynamics”, *Annals Phys.* **394** (2018) 50–72, arXiv:1711.02496 [nucl-th].
- [44] Y. Jiang, S. Shi, Y. Yin, and J. Liao, “Quantifying the chiral magnetic effect from anomalous-viscous fluid dynamics”, *Chin. Phys. C* **42** no. 1, (2018) 011001, arXiv:1611.04586 [nucl-th].
- [45] S. Shi, H. Zhang, D. Hou, and J. Liao, “Signatures of Chiral Magnetic Effect in the Collisions of Isobars”, *Phys. Rev. Lett.* **125** (2020) 242301, arXiv:1910.14010 [nucl-th].
- [46] **ALICE** Collaboration, K. Aamodt *et al.*, “The ALICE experiment at the CERN LHC”, *JINST* **3** (2008) S08002.
- [47] **ALICE** Collaboration, B. B. Abelev *et al.*, “Performance of the ALICE Experiment at the CERN LHC”, *Int. J. Mod. Phys. A* **29** (2014) 1430044, arXiv:1402.4476 [nucl-ex].
- [48] **ALICE** Collaboration, K. Aamodt *et al.*, “Alignment of the ALICE Inner Tracking System with cosmic-ray tracks”, *JINST* **5** (2010) P03003, arXiv:1001.0502 [physics.ins-det].
- [49] J. Alme *et al.*, “The ALICE TPC, a large 3-dimensional tracking device with fast readout for ultra-high multiplicity events”, *Nucl. Instrum. Meth. A* **622** (2010) 316–367, arXiv:1001.1950 [physics.ins-det].
- [50] **ALICE** Collaboration, E. Abbas *et al.*, “Performance of the ALICE VZERO system”, *JINST* **8** (2013) P10016, arXiv:1306.3130 [nucl-ex].

- [51] R. Arnaldi *et al.*, “The zero degree calorimeters for the ALICE experiment”, *Nucl. Instrum. Meth. A* **581** (2007) 397–401. [Erratum: *Nucl.Instrum.Meth.A* 604, 765 (2009)].
- [52] ALICE Collaboration, S. Acharya *et al.*, “Centrality determination using the Glauber model in Xe–Xe collisions at $\sqrt{s_{NN}} = 5.44$ TeV”, *ALICE-PUBLIC-2018-003* (2018) 1–23. <http://cds.cern.ch/record/2315401>.
- [53] ALICE Collaboration, S. Acharya *et al.*, “Transverse momentum spectra and nuclear modification factors of charged particles in Xe–Xe collisions at $\sqrt{s_{NN}} = 5.44$ TeV”, *Phys. Lett. B* **788** (2019) 166–179, arXiv:1805.04399 [nucl-ex].
- [54] X.-N. Wang and M. Gyulassy, “HIJING: A Monte Carlo model for multiple jet production in pp, pA and AA collisions”, *Phys. Rev.* **D44** (1991) 3501–3516.
- [55] M. Gyulassy and X.-N. Wang, “HIJING 1.0: A Monte Carlo program for parton and particle production in high-energy hadronic and nuclear collisions”, *Comput. Phys. Commun.* **83** (1994) 307, arXiv:nucl-th/9502021.
- [56] R. Brun *et al.*, “GEANT Detector Description and Simulation Tool”, *CERN-W5013* **1** (1994) 1. <https://cds.cern.ch/record/1082634>.
- [57] U. Gürsoy, D. Kharzeev, E. Marcus, K. Rajagopal, and C. Shen, “Charge-dependent Flow Induced by Magnetic and Electric Fields in Heavy Ion Collisions”, *Phys. Rev. C* **98** no. 5, (2018) 055201, arXiv:1806.05288 [hep-ph].
- [58] ATLAS Collaboration, G. Aad *et al.*, “Longitudinal Flow Decorrelations in Xe+Xe Collisions at $\sqrt{s_{NN}} = 5.44$ TeV with the ATLAS Detector”, *Phys. Rev. Lett.* **126** no. 12, (2021) 122301, arXiv:2001.04201 [nucl-ex].
- [59] I. Selyuzhenkov and S. Voloshin, “Effects of non-uniform acceptance in anisotropic flow measurement”, *Phys. Rev. C* **77** (2008) 034904, arXiv:0707.4672 [nucl-th].
- [60] ALICE Collaboration, S. Acharya *et al.*, “Transverse momentum spectra and nuclear modification factors of charged particles in pp, p–Pb and Pb–Pb collisions at the LHC”, *JHEP* **11** (2018) 013, arXiv:1802.09145 [nucl-ex].
- [61] R. Barlow, “Systematic errors: Facts and fictions”, in *Conference on Advanced Statistical Techniques in Particle Physics*, pp. 134–144. 7, 2002. arXiv:hep-ex/0207026.
- [62] ALICE Collaboration, J. Adam *et al.*, “Centrality dependence of the charged-particle multiplicity density at midrapidity in Pb–Pb collisions at $\sqrt{s_{NN}} = 5.02$ TeV”, *Phys. Rev. Lett.* **116** no. 22, (2016) 222302, arXiv:1512.06104 [nucl-ex].
- [63] ALICE Collaboration, S. Acharya *et al.*, “Centrality and pseudorapidity dependence of the charged-particle multiplicity density in Xe–Xe collisions at $\sqrt{s_{NN}} = 5.44$ TeV”, *Phys. Lett. B* **790** (2019) 35–48, arXiv:1805.04432 [nucl-ex].
- [64] F. Retiere and M. A. Lisa, “Observable implications of geometrical and dynamical aspects of freeze out in heavy ion collisions”, *Phys. Rev.* **C70** (2004) 044907, arXiv:nucl-th/0312024.
- [65] ALICE Collaboration, S. Acharya *et al.*, “Production of pions, kaons, (anti-)protons and ϕ mesons in Xe–Xe collisions at $\sqrt{s_{NN}} = 5.44$ TeV”, arXiv:2101.03100 [nucl-ex].
- [66] ALICE Collaboration, S. Acharya *et al.*, “Anisotropic flow of identified hadrons in Xe–Xe collisions at $\sqrt{s_{NN}} = 5.44$ TeV”, *JHEP* **10** (2021) 152, arXiv:2107.10592 [nucl-ex].

- [67] H. Song and U. W. Heinz, “Suppression of elliptic flow in a minimally viscous quark-gluon plasma”, *Phys. Lett. B* **658** (2008) 279–283, arXiv:0709.0742 [nucl-th].
- [68] S. A. Bass *et al.*, “Microscopic models for ultrarelativistic heavy ion collisions”, *Prog. Part. Nucl. Phys.* **41** (1998) 255–369, arXiv:nucl-th/9803035.
- [69] M. Bleicher *et al.*, “Relativistic hadron–hadron collisions in the ultrarelativistic quantum molecular dynamics model”, *J. Phys. G* **25** (1999) 1859–1896, arXiv:hep-ph/9909407.
- [70] M. L. Miller, K. Reygers, S. J. Sanders, and P. Steinberg, “Glauber modeling in high energy nuclear collisions”, *Ann. Rev. Nucl. Part. Sci.* **57** (2007) 205–243, arXiv:nucl-ex/0701025.
- [71] ALICE Collaboration, S. Acharya *et al.*, “Centrality determination in heavy ion collisions”, *ALICE-PUBLIC-2018-011* (2018) 1–28. <https://cds.cern.ch/record/2636623>.
- [72] J. S. Moreland, J. E. Bernhard, and S. A. Bass, “Alternative ansatz to wounded nucleon and binary collision scaling in high-energy nuclear collisions”, *Phys.Rev.* **C92** no. 1, (2015) 011901, arXiv:1412.4708 [nucl-th].
- [73] W.-T. Deng, X.-G. Huang, G.-L. Ma, and G. Wang, “Test the chiral magnetic effect with isobaric collisions”, *Phys. Rev. C* **94** (2016) 041901, arXiv:1607.04697 [nucl-th].